J. Fluid Mech. (2019), *vol.* 877, R3, doi:10.1017/jfm.2019.651

JFM RAPIDS
journals.cambridge.org/rapids



Third-order structure functions for isotropic turbulence with bidirectional energy transfer

Jin-Han Xie[1,†] **and Oliver Bühler**[1]

[1]Courant Institute of Mathematical Sciences, New York University, New York, NY 10012, USA

(Received 23 May 2019; revised 28 July 2019; accepted 6 August 2019;
first published online 2 September 2019)

We derive and test a new heuristic theory for third-order structure functions that resolves the forcing scale in the scenario of simultaneous spectral energy transfer to both small and large scales, which can occur naturally, for example, in rotating stratified turbulence or magnetohydrodynamical (MHD) turbulence. The theory has three parameters – namely the upscale/downscale energy transfer rates and the forcing scale – and it includes the classic inertial-range theories as local limits. When applied to measured data, our global-in-scale theory can deduce the energy transfer rates using the full range of data, therefore it has broader applications compared with the local theories, especially in situations where the data is imperfect. In addition, because of the resolution of forcing scales, the new theory can detect the scales of energy input, which was impossible before. We test our new theory with a two-dimensional simulation of MHD turbulence.

Key words: turbulence theory, isotropic turbulence, MHD turbulence

1. Introduction

The direction of spectral energy transfer is a crucial feature of a turbulent system. In contrast to isotropic two- and three-dimensional turbulence, where the spectral energy transfer is predominantly to large or small scales (Kolmogorov 1941; Kraichnan 1982), some systems such as thin-layer turbulence (Celani, Musacchio & Vincenzi 2010; Benavides & Alexakis 2017) exhibit more complex behaviour, where the energy transfer can be bidirectional. (In Alexakis & Biferale (2018) this scenario is termed a 'split energy cascade', but we think 'bidirectional energy transfer' is more intuitive.) Alexakis & Biferale (2018) provide a relevant review article covering this and other physical situations.

To quantify the magnitude and the direction of energy transfer, theories that link the measurable third-order structure functions to energy fluxes have been developed in the inertial ranges, which are away from both the dissipation and forcing scales

† Email address for correspondence: jhxie@cims.nyu.edu

© Cambridge University Press 2019

https://doi.org/10.1017/jfm.2019.651 Published online by Cambridge University Press

for isotropic turbulent systems. For example, in three-dimensional (3-D) isotropic turbulence, where energy transfers downscale, Kolmogorov (1941) found that the longitudinal third-order structure function $\overline{\delta u_L^3}$ and the energy input rate ϵ, which equals the magnitude of energy flux in a statistically steady state, are exactly related by $\overline{\delta u_L^3} = -\frac{4}{5}\epsilon r < 0$, where r is the distance between the two measured points in the inertial range. In contrast, energy transfers to large scales in two-dimensional (2-D) turbulence, and the corresponding relation in the energy inertial range becomes $\overline{\delta u_L^3} = \frac{3}{2}\epsilon r > 0$ (Bernard 1999; Lindborg 1999; Yakhot 1999). It has since become commonplace to use local fits to power laws of observed third-order structure functions to detect spectral energy transfer directions in a variety of numerical and experimental systems (Kurien, L & Wingate 2006; Lindborg 2007; Byrne, Xia & Shats 2011; Deusebio, Augier & Lindborg 2014), including the solar wind (Sorriso-Valvo *et al.* 2007), atmospheric flow (Cho & Lindborg 2001; Byrne & Zhang 2013) and Jupiter's weather layer (Young & Read 2017). Indeed, sometimes just the sign of the observed third-order structure function has been used to estimate the direction of the energy flux at some scale r. This is not a robust diagnostic once we consider the shortcomings of the local theories.

First, they are valid only in local inertial ranges, which are far away from both the forcing and dissipation scales. Thus, when applying to measured data, one has to determine where the inertial range is in the first place – that is, in order to use the Kolmogorov (1941) theory one needs to find where the third-order structure function is linear in r. But it is possible that different researchers choose different data ranges, and inertial ranges might be short and hard to identify using imperfect measured data, all of which leads to uncertainties. Second, the local, inertial-range theories by definition fail at the forcing scales, which prevents the important detection of forcing scales (for example, for geophysical flows). Third, previous theories were developed for scenarios with unidirectional energy transfer, but there is good evidence that in natural turbulence (for example, in the atmosphere and oceans), energy transfers simultaneously to both large and small scales (Marino, Pouquet & Rosenberg 2015; Pouquet *et al.* 2017). The direction of energy flux is essential for these structure-function theories – for example, Xie & Bühler (2018) illustrate how the 3-D (Kolmogorov 1941) and 2-D (Kraichnan 1982) turbulence must be treated differently when taking the infinite-Reynolds-number limit in the Kármán–Howarth–Monin (KHM) (see Monin & Yaglom 1975; Frisch 1995) equation, because of their opposite directions of energy transfer. So it is questionable to directly apply the previous theories to scenarios with bidirectional energy transfer.

Thus, we want to obtain a forcing-resolving global-in-scale theory that not only captures different inertial ranges in one formula, but also applies to bidirectional energy transfer, allowing us to make use of the measured data over a wide range that includes the forcing scales. Here, we derive such a theory for isotropic 2-D turbulence and test it against a numerical simulation of 2-D MHD turbulence with bidirectional energy transfer (Seshasayanan, Benavides & Alexakis 2014; Seshasayanan & Alexakis 2016), which is a limiting case of 3-D MHD with a strong background magnetic field (Gallet & Doering 2015). We also show how to adapt our theory to turbulent flows in one or three dimensions.

2. Theoretical framework

We start from the generic Kármán–Howarth–Monin (KHM) equation for two-point correlations, in which the nonlinear terms appear via the divergence of a third-order

https://doi.org/10.1017/jfm.2019.651 Published online by Cambridge University Press

vector field:

$$\frac{1}{2}\frac{\partial}{\partial t}C - \frac{1}{4}\boldsymbol{\nabla}\cdot\boldsymbol{V} = D + P. \tag{2.1}$$

Here C is the second-order correlation function, $\boldsymbol{V}$ is a vector of third-order structure functions if the system has a quadratic nonlinearity, and D and P describe the effects of dissipation and external forcing, respectively. For example, in the case of 2-D homogeneous isotropic turbulence studied by Xie & Bühler (2018),

$$C = \overline{\boldsymbol{u}\cdot\boldsymbol{u}'}, \tag{2.2a}$$
$$\boldsymbol{V} = \overline{\delta\boldsymbol{u}|\delta\boldsymbol{u}|^2}, \tag{2.2b}$$
$$D = -\alpha\overline{\boldsymbol{u}\cdot\boldsymbol{u}'} + \nu\nabla^2\overline{\boldsymbol{u}\cdot\boldsymbol{u}'}, \tag{2.2c}$$
$$P = \tfrac{1}{2}(\overline{\boldsymbol{F}\cdot\boldsymbol{u}'} + \overline{\boldsymbol{F}'\cdot\boldsymbol{u}}), \tag{2.2d}$$

where $\boldsymbol{u}' = \boldsymbol{u}(\boldsymbol{x}+\boldsymbol{r})$, with $\boldsymbol{r}$ the displacement between two measurement points, $\delta\boldsymbol{u} = \boldsymbol{u}' - \boldsymbol{u}$, α is a Rayleigh damping rate, ν is the viscosity, $\boldsymbol{F}$ is the external forcing and the overline denotes the ensemble average. For statistically steady turbulent states, (2.1) simplifies to

$$-\tfrac{1}{4}\boldsymbol{\nabla}\cdot\boldsymbol{V} = D + P. \tag{2.3}$$

The Fourier transform of C yields the power spectrum as a function of wavenumber $\boldsymbol{k}$ so, by applying the Fourier transform to (2.1) and integrating over the wavenumber shell $|\boldsymbol{k}| < K$, it follows that (see § 6 in Frisch 1995)

$$F(K) = -\int_{|\boldsymbol{k}|\leqslant K} \frac{1}{4}\widehat{\boldsymbol{\nabla}\cdot\boldsymbol{V}}\,\mathrm{d}\boldsymbol{k}, \tag{2.4}$$

is the nonlinear spectral energy transfer rate across the wavenumber shell with radius K; that is, a positive $F(K) > 0$ measures the downscale energy transfer from larger scales ($|\boldsymbol{k}| < K$) to smaller scales ($|\boldsymbol{k}| > K$) in spectral space. Under the assumption of isotropy, the third-order structure-function vector is

$$\boldsymbol{V} = V(r)\hat{\boldsymbol{r}}, \tag{2.5}$$

where $r = |\boldsymbol{r}|$ and $\hat{\boldsymbol{r}}$ is a unit vector pointing in the direction of $\boldsymbol{r}$. Thus, in two dimensions (2.4) can be expressed as (see (5.8) in Xie & Bühler (2018))

$$F(K) = -\frac{K^2}{4}\int_0^\infty V(r)\mathrm{J}_2(Kr)\,\mathrm{d}r, \tag{2.6}$$

where J_2 is the second-order Bessel function. Equivalently, using the orthogonality of Bessel functions and the robust convergence of $V(r)$ for large distances r, we can invert (2.6) to obtain

$$V(r) = -4r\int_0^\infty \frac{1}{K}F(K)\mathrm{J}_2(Kr)\,\mathrm{d}K. \tag{2.7}$$

https://doi.org/10.1017/jfm.2019.651 Published online by Cambridge University Press

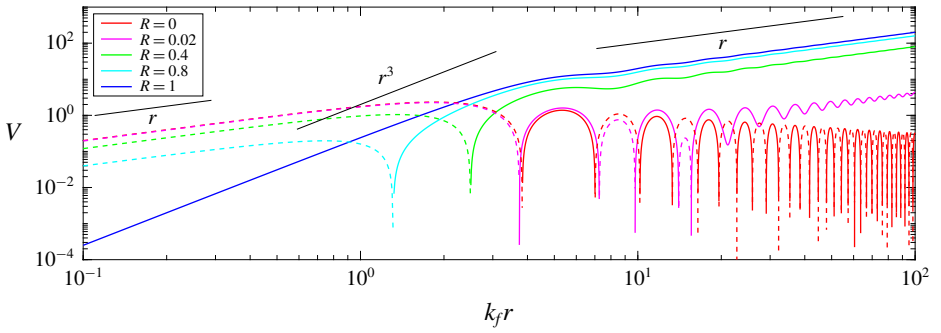


FIGURE 1. Theoretical expression (2.9) with $k_f = 1$, $\epsilon = 1$ and different values of $R \equiv \epsilon_u/\epsilon$. At the right end ($k_f r = 10^2$), the curves align with descending R from above to below. Solid and dashed lines denote positive and negative values, respectively. The black lines illustrate classical power laws.

2.1. *Non-dissipative theory*

We now consider first an idealized non-dissipative scenario where the external forcing is sharply localized at some wavenumber k_f with corresponding length scale $l_f = 1/k_f$, whilst the dissipation at small and large scales has been pushed to $K \to \infty$ and $K \to 0$, respectively. Corrections due to finite-scale dissipation are deferred until § 2.2. Therefore, at finite K we can argue that $F(K)$ must take the piecewise constant form

$$F(K) = -\epsilon_u + (\epsilon_u + \epsilon_d)H(K - k_f). \tag{2.8}$$

Here ϵ_u and ϵ_d are the magnitudes of upscale and downscale energy fluxes, H is the Heaviside function, and $\epsilon = \epsilon_u + \epsilon_d$ is the total energy input rate. Substituting (2.8) into (2.7) yields the corresponding non-dissipative expression

$$V(r) = 2\epsilon_u r - 4\frac{\epsilon}{k_f}\mathrm{J}_1(k_f r), \tag{2.9}$$

which extends Kolmogorov's classical inertial-range theory by including the forcing scale as well as bidirectional energy transfer. In contrast to the classic definition of inertial range, we do not assume that the considered scale r is far away from the forcing scale l_f; thus, (2.9) is a forcing-scale-resolving expression and we call it a global solution. This new expression generalizes previous forcing-scale-resolving results with total upscale (see Xie & Bühler (2018)) and downscale (see Xie & Bühler (2019)) energy transfer by capturing the bidirectional energy transfer. We illustrate its behaviour in figure 1 using $k_f = 1$, $\epsilon = 1$, and various values of the fractional upscale flux $R = \epsilon_u/\epsilon$. In the limit $R = 1$ of completely upscale energy flux, the present (2.9) reduces to the second equality in (4.9), already derived in Xie & Bühler (2018). Notably, $V(r)$ is sign-definite and positive only if $R = 1$; that is, for all values $R < 1$, the sign of $V(r)$ changes at least once. Also, the case with $R = 0.02$ is almost indistinguishable from the limiting case $R = 0$ for downward-only energy flux, but only if $k_f r \ll 10$. Otherwise their difference becomes obvious as $k_f r \gg 10$. In the intermediate range ($k_f r \sim 10$), where r is larger than the forcing scale $1/k_f$ and almost all energy transfers upscale, the structure function V with $R = 0.02$ still has alternating signs, which illustrates once more that one cannot safely read off

https://doi.org/10.1017/jfm.2019.651 Published online by Cambridge University Press

the direction of the spectral transfer just from the sign of the third-order structure function.

Naturally, in the limits of large and small $k_f r$ the global expression (2.9) recovers the classic local results (see Bernard 1999; Lindborg 1999; Yakhot 1999) asymptotically:

$$V(r) = \begin{cases} \underbrace{-2\epsilon_d r}_{\textit{downscale energy}} + \underbrace{\tfrac{1}{4}\epsilon k_f^2 r^3}_{\textit{'enstrophy'}} + O((k_f r)^5), & \text{when } k_f r \ll 1, \\ \underbrace{2\epsilon_u r}_{\textit{upscale energy}} + O((k_f r)^{-1/2}), & \text{when } k_f r \gg 1. \end{cases} \tag{2.10}$$

Interestingly, the small-scale 'enstrophy' term recovers the classical enstrophy cascade result of 2-D turbulence when $\epsilon_d = 0$, but if $\epsilon_d \neq 0$ there may be not even be any enstrophy conservation in the turbulent system, but nonetheless this term arises in all cases in the expansion of $V(r)$.

2.2. *Dissipative corrections*

For realistic turbulence, dissipation brings about corrections to (2.9) at large and small r. For example, in 2-D turbulence a linear Ekman damping introduces the log-correlation to the energy spectrum at the enstrophy inertial range (Kraichnan 1971), and it bounds the range of inverse energy cascade (for example, Smith *et al.* 2002). We do not want to introduce a closure that links second- and third-order structure functions to calculate the shape of them; instead, we simply derive an exact relation that links them diagnostically. The derivation starts from distinguishing the large- and small-scale damping terms which dominantly absorb upscale and downscale energy fluxes, respectively. This distinction is necessary because the two types of damping influence the inertial range differently in the limit of zero viscosity: the large-scale damping brings about a leading-order contribution while the effect of small-scale damping is of higher order compared with that of the external forcing, as shown in Xie & Bühler (2018). Let us write the dissipation term in (2.1) as

$$D = \mathcal{L}_D C = D_l + D_s = \mathcal{L}_{Dl} C + \mathcal{L}_{Ds} C, \tag{2.11}$$

where the operator $\mathcal{L}_D$ is the sum of large- and small-scale parts $\mathcal{L}_{Dl}$ and $\mathcal{L}_{Ds}$, respectively. For example, Xie & Bühler (2018) used $\mathcal{L}_{Dl} = -\alpha$ and $\mathcal{L}_{Ds} = \nu\nabla^2$ for Rayleigh damping and Navier–Stokes diffusion. The large- and small-scale net dissipation rates are then $\epsilon_u = D_l|_{r=0}$ and $\epsilon_d = D_s|_{r=0}$, respectively. For two-dimensional isotropic turbulence, integrating (2.3) over a disk of radius r yields

$$V_d(r) = -\frac{4}{r}\int_0^r sD_s(s)\,\mathrm{d}s - \frac{4}{r}\int_0^r s(D_l(s)+\epsilon_u)\,\mathrm{d}s + 2\epsilon_u r - \frac{4}{r}\int_0^r sP(s)\,\mathrm{d}s. \tag{2.12}$$

If the external forcing is white-noise in time and centred at wavenumber k_f then (2.12) becomes

$$V_d = -\frac{4}{r}\int_0^r sD_s(s)\,\mathrm{d}s - \frac{4}{r}\int_0^r s(D_l(s)+\epsilon_u)\,\mathrm{d}s + 2\epsilon_u r - 4\frac{\epsilon}{k_f}\mathrm{J}_1(k_f r). \tag{2.13}$$

This is the sought-after dissipative correction to (2.9). We need to note that for a general 2-D turbulence system we are not able to strictly derive that in the limit

https://doi.org/10.1017/jfm.2019.651 Published online by Cambridge University Press

of zero viscosity the finite damping effect tends to zero and is therefore negligible compared with the limit result, and to do so we need to consider a specific turbulence system with a prescribed damping term; one such example is 2-D turbulence studied by Xie & Bühler (2018). Note that in the derivation we need to distinguish large- and small-scale dissipations. But the smallness of the finite damping effect in the zero-viscosity limit matches the derivation starting from the idealized spectral energy flux (2.8). In the next section we check both the non-dissipative result (2.9) and its dissipation correction (2.13) in a MHD example.

3. Application to two-dimensional MHD turbulence

To test our heuristic theory we performed numerical simulations of a 2-D MHD turbulent flow in which the velocity $\boldsymbol{v}$ and the magnetic field $\boldsymbol{B}$ are coplanar. This is an ideal test system because Seshasayanan *et al.* (2014) found bidirectional energy transfer in this 2-D system, and also its KHM equation has the generic form (2.1) with a third-order structure-function vector (see Podesta 2008) defined by

$$\boldsymbol{V} = \overline{\delta\boldsymbol{u}(\delta\boldsymbol{u}\cdot\delta\boldsymbol{u})} + \overline{\delta\boldsymbol{u}(\delta\boldsymbol{B}\cdot\delta\boldsymbol{B})} - 2\overline{\delta\boldsymbol{B}(\delta\boldsymbol{B}\cdot\delta\boldsymbol{u})}. \tag{3.1}$$

Here the magnetic field is normalized to have velocity units such that $C = \overline{\boldsymbol{u}\cdot\boldsymbol{u}'} + \overline{\boldsymbol{B}\cdot\boldsymbol{B}'}$.

The numerical simulation uses a Fourier pseudospectral method with 2/3 dealiasing in space, a resolution 512×512 and a fourth-order explicit Runge–Kutta scheme in time, in which the nonlinear terms are treated explicitly and linear terms implicitly using an integrating factor method. We take the forcing wavenumber to be $k_f = 32$, the momentum and magnetic equation are forced by random forces which are white-noise in time, and we control the kinetic energy input rate to be 100 times that of the magnetic energy, which is a case that is found to have bidirectional energy transfer (Seshasayanan & Alexakis 2016). We add hypoviscosity with operator ∇^{-2} and hyperviscosity with operator ∇^6 to both the velocity and magnetic fields to dissipate energy transferred to large and small scales, respectively, and therefore the turbulence system reaches a statistically steady state.

We show in figure 2(*a*) the spectral transfer $F(K)$ of total energy, which is the sum of kinetic and magnetic energy. Here the spectral energy transfer is directly calculated in Fourier space from the pseudospectral code without making use of the third-order structure function in physical space. As expected, bidirectional energy transfer is observed: around 60 % of total energy transfers upscale and is mainly dissipated by the hypoviscosity, while the other 40 % transfers downscale and is mainly dissipated by the hyperviscosity; this corresponds to $R \approx 0.6$. In table 1 the value of ϵ_u is obtained by calculating the amount of energy dissipated by the hypoviscosity and the value of ϵ is calculated from the white-noise forcing applied in the numerical simulation.

Now, figure 2(*b*) shows the comparison of structure functions obtained in several different ways. The blue curve shows the structure function directly measured from the statistics of the velocity and magnetic fields. The black curve is the theoretical formula (2.9) using the observed value of ϵ_u as well as the forcing wavenumber $k_f = 32$ and the total energy transfer ϵ known from the numerical set-up. The red curve is a least-square fitting of the theoretical result (2.9) using only the four measured points from the blue curve marked in green squares. We choose these four points as a test because we need to capture the sign transition of the third-order structure function and

https://doi.org/10.1017/jfm.2019.651 Published online by Cambridge University Press

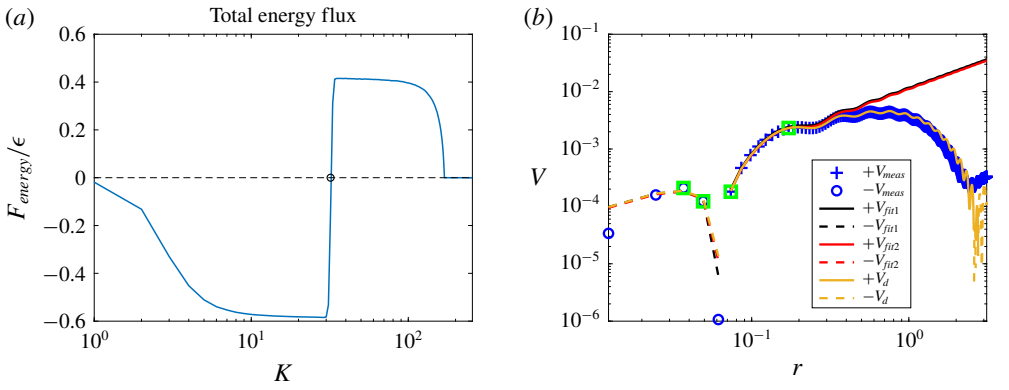


FIGURE 2. (*a*) Total observed energy transfer normalized by the total energy input rate ϵ. The circle marks the forcing wavenumber $k_f = 32$. (*b*) Comparison of third-order structure functions obtained from the statistics of numerical data (blue), two zero-viscosity fitting curves (black and red), and the finite damping fitting curve (yellow). The four green boxes mark the four points used for fitting 2 (red). In the legend, the symbols '+' and '−' denote positive and negative values, respectively.

	ϵ	$R = \epsilon_u/\epsilon$	k_f
V_{fit1}	1.000×10^{-2}	0.5845	32.00
V_{fit2}	0.958×10^{-2}	0.5786	32.06

TABLE 1. Comparison of coefficients of two fitting curves shown in figure 2(*b*).

we intentionally avoid choosing points in the classic inertial ranges to distinguish our theory from the past ones: the left three points are around the region of sign change and the last point is around the forcing scale. The parameters used in the fittings are also shown in table 1. This comparison shows that the fitting based on our global theory using only four measured structure-function values works well in determining the bidirectional energy flux rate within a 5 % error.

Figure 2(*b*) also shows that the dissipation at large scale due to hypoviscosity brings about a non-negligible discrepancy between the theory (2.9) in the zero-viscosity limit and the numerical data. To capture this large-scale dissipative correction we include the hypoviscosity $\mathcal{L}_{Dl} = \alpha\nabla^{-2}$ but omit the hyperviscosity effect in (2.13) to obtain the viscous expression of the third-order structure function

$$\begin{aligned} V_d &= -\frac{4}{r}\int_0^r s(\alpha\nabla^{-2}(\overline{\boldsymbol{u}\cdot\boldsymbol{u}'}(s) + \overline{\boldsymbol{B}\cdot\boldsymbol{B}'}(s)) - \epsilon_u)\,\mathrm{d}s + 2\epsilon_u r - \frac{4\epsilon}{k_f}\mathrm{J}_1(k_f r) \\ &= -\frac{2\alpha}{r}\int_0^r s(\overline{\delta\psi^2}(s) + \overline{\delta A^2}(s))\,\mathrm{d}s + 2\epsilon_u r - \frac{4\epsilon}{k_f}\mathrm{J}_1(k_f r), \end{aligned} \tag{3.2}$$

where ψ and A are the stream functions for $\boldsymbol{u}$ and $\boldsymbol{B}$, respectively, and we have used the identity $\nabla^2\overline{AA'} = -\overline{\nabla A\cdot\nabla' A'}$, which holds for arbitrary scalar fields A with isotropic statistics. The excellent match between (3.2) and the numerical data verifies the validity of (2.13). Thus, if the damping form is known and the corresponding second-order structure function can be measured, we can make use of them to fit the data in a broader range to detect energy transfer.

https://doi.org/10.1017/jfm.2019.651 Published online by Cambridge University Press

4. Discussion

To test our global results (2.9) and (2.13), we deliberately used a relatively low-resolution 2-D MHD simulation, which provides imperfect inertial ranges. This severely limits the applicability of classic local theories, but not of the new global theory. Indeed, due to the limited resolution, the direct numerical data (blue) shows that the energy inertial ranges which have $V \sim r$ behaviour are not observed. Similarly, because of the non-negligible influence from the forcing scale, a straight line corresponding to $V \sim r^3$ is also not clear. These make the traditional process based on classic local theories of fitting straight lines in a log–log plot to obtain the information of energy flux impossible, but our global theory can achieve it. In addition, since our global theory only contains three parameters and applies to a broader range containing the forcing scale, we can make use of more data information and thereby detect the forcing scale.

The sublimits of our global expression (2.9) match those of the classic inertial-range results (see (2.10)), implying that our theory captures the transitions of inertial ranges. Also, it implies that simply 'gluing' the theories of different inertial ranges for turbulence with unidirectional energy transfer to obtain a global theory is fallacious, because the constant in front of the r^3 depends on the total energy input instead of the upscale transferred energy alone. Also, this expansion brings about a new perspective to understanding the 'enstrophy' range. In Kraichnan (1982)'s argument, the simultaneous conservation of both energy and enstrophy results in an upscale energy transfer and a downscale enstrophy transfer, and correspondingly in the enstrophy inertial range the third-order structure function has an r^3 dependence. However, our theory shows that as long as there exists non-zero upscale energy transfer, an r^3 dependence of the third-order structure function exists as a natural consequence of asymptotic expansion, but the presence of a constant downscale 'enstrophy' flux is not necessary with the 'enstrophy', a preserved quantity without external force and dissipation, which is the case for 2-D MHD turbulence.

In this paper, we present a general framework for the inertial-range third-order structure-function global theory that captures bidirectional energy transfer and resolves the forcing scale in homogeneous isotropic turbulence. This theory has three parameters, ϵ_u, ϵ_d and l_f, that describe the upscale energy flux magnitude, downscale energy flux magnitude and the forcing scale. The classic local theories that are applicable away from the forcing scales are recovered as sublimits of this global theory, which captures the transitions as well.

In the present theory we assumed that the energy input is δ-centred at one wavenumber k_f, but considering that when assuming a δ-centred external forcing we are solving a Green's function for equation (2.3) we can express the expression of the third-order structure function with a general distribution of the energy input rate after a convolution. Thus, our theory can be used to detect the unknown distribution of energy input for a 2-D turbulent system.

As to the finite damping effect, it is shown in Xie & Bühler (2018) that for 2-D turbulence with damping operator $\mathcal{L}_D = -\alpha + \nu\nabla^2$, the damping effect in (2.13) tends to zero as α and ν tend to zero. But the comparable smallness of the damping effect in (2.13) remains to be studied carefully in other turbulence systems. And it is important to justify that the different operations to the large- and small-scale damping effects are general, and therefore in the limit of zero-viscosity, large-scale damping impacts the third-order structure function at the leading order while the influence of small-scale damping is negligible.

https://doi.org/10.1017/jfm.2019.651 Published online by Cambridge University Press

In the main text of this paper we only show the 2-D theory for the reason that we can test it numerically. We close the paper by presenting the third-order structure-function expression analogous to (2.9) for one-dimensional (1-D) (Burgers) and 3-D isotropic turbulence with bidirectional energy transfer:

$$\begin{aligned}\text{1-D:}\quad V &= 4\epsilon_u r - 4\epsilon\frac{\sin(k_f r)}{k_f}\\ &= \begin{cases} -4\epsilon_d r + \dfrac{2}{3}\epsilon k_f^2 r^3 + O((k_f r)^5), & (k_f r \ll 1),\\ 4\epsilon_u r + O(1), & (k_f r \gg 1).\end{cases}\end{aligned} \tag{4.1}$$

$$\begin{aligned}\text{3-D:}\quad V &= \frac{4}{3}\epsilon_u r - 4\epsilon\frac{\sin(k_f r) - Kr\cos(k_f r)}{k_f^3 r^2}\\ &= \begin{cases} -\dfrac{4}{3}\epsilon_d r + \dfrac{2}{15}\epsilon k_f^2 r^3 + O((k_f r)^5), & (k_f r \ll 1),\\ \dfrac{4}{3}\epsilon_u r + O((k_f r)^{-1}), & (k_f r \gg 1).\end{cases}\end{aligned} \tag{4.2}$$

Note that the 3-D result for small $k_f r$ gives $V = -\frac{4}{3}\epsilon_d r$. For classic 3-D turbulence, considering the relation between V and the longitudinal third-order structure function

$$V = \overline{\delta u_L^3} + \frac{1}{3}\frac{\mathrm{d}}{\mathrm{d}r}(r\overline{\delta u_L^3}), \tag{4.3}$$

we recover the $-4/5$ law of Kolmogorov (1941)'s theory: $\overline{\delta u_L^3} = -\frac{4}{5}\epsilon_d r$. The detailed derivations of the 1-D and 3-D expressions are shown in appendix A.

Acknowledgements

We are grateful to A. Majda and S. Smith for discussions that helped to improve this paper. We gratefully acknowledge financial support from the United States National Science Foundation grants DMS-1312159 and DMS-1813891 and also Office of Naval Research grants N00014-15-1-2355 and N00014-19-1-2407.

Appendix A. Derivation of the expressions of third-order structure functions in one and three dimensions

The key to deriving the expressions of third-order structure functions is obtaining the relation between the structure function and the energy flux, using, for example, (2.7) in the main text, then we substitute the idealized energy flux function (see (2.8) in the main text) to obtain the final result. In this section we apply this procedure to 1-D and 3-D turbulence to obtain the expressions (4.1) and (4.2) in the main text.

A.1. *Third-order structure function in one dimension*

In one dimension, the spectral energy flux (2.4) can be expressed as

$$F(K) = -\frac{1}{2\pi}\int_{-K}^{K}\mathrm{d}k\int_{-\infty}^{\infty}\mathrm{d}s\frac{1}{4}\frac{\mathrm{d}V}{\mathrm{d}s}\mathrm{e}^{\mathrm{i}ks}, \tag{A 1}$$

therefore

$$\frac{\mathrm{d}F}{\mathrm{d}K} = -\frac{1}{4\pi}\int_{-\infty}^{\infty}\mathrm{d}s\frac{\mathrm{d}V}{\mathrm{d}s}\mathrm{e}^{\mathrm{i}Ks}. \tag{A 2}$$

https://doi.org/10.1017/jfm.2019.651 Published online by Cambridge University Press

Taking the inverse Fourier transform to (A 2) we obtain

$$\frac{\mathrm{d}V}{\mathrm{d}r} = -2\int_{-\infty}^{\infty} \mathrm{d}K \frac{\mathrm{d}F}{\mathrm{d}K} \mathrm{e}^{-\mathrm{i}Kr}, \tag{A 3}$$

so

$$V = 4\int_0^{\infty} \mathrm{d}K\, F \frac{Kr\cos(Kr) - \sin(Kr)}{K^2}, \tag{A 4}$$

which expresses V as a functional of F. Thus, substituting the idealized expression for the bidirectional energy flux

$$F = -\epsilon_u + (\epsilon_u + \epsilon_d)H(K - k_f) \tag{A 5}$$

into (A 4) we obtain

$$V = 4\epsilon_u r - 4\epsilon \frac{\sin(k_f r)}{k_f}, \tag{A 6}$$

which is (4.1).

A.2. *Third-order structure function in three dimensions*

In three dimensions, the spectral energy flux (2.4) can be expressed as

$$F(K) = -\frac{1}{(2\pi)^3}\int_0^K \mathrm{d}k \int_0^{\pi} \mathrm{d}\phi \int_0^{\pi} \mathrm{d}\theta k^2 \sin(\phi) \int_{-\infty}^{\infty}\int_{-\infty}^{\infty}\int_{-\infty}^{\infty} \mathrm{d}\boldsymbol{r} \frac{1}{4}\boldsymbol{\nabla}\cdot\boldsymbol{V}\mathrm{e}^{\mathrm{i}\boldsymbol{k}\cdot\boldsymbol{r}}, \tag{A 7}$$

therefore under the assumption of isotropy, taking the K-derivative and inverse Fourier transform we obtain

$$\frac{1}{r^2}\frac{\mathrm{d}}{\mathrm{d}r}(r^2 V) = -4\int_0^{\infty} \mathrm{d}K \frac{\mathrm{d}F}{\mathrm{d}K}\frac{\sin(Kr)}{Kr}. \tag{A 8}$$

So we can integrate (A 8) to obtain

$$V = 4\int_0^{\infty} \mathrm{d}K\, F \frac{2Kr - 3\sin(Kr) + Kr\cos(Kr)}{K^4 r^3}. \tag{A 9}$$

Thus, substituting the idealized expression for the bidirectional energy flux (A 5) into (A 9) we obtain

$$V = \frac{4}{3}\epsilon_u r - 4\epsilon \frac{\sin(k_f r) - Kr\cos(k_f r)}{k_f^3 r^2}, \tag{A 10}$$

which is (4.2).

References

Alexakis, A. & Biferale, L. 2018 Cascades and transitions in turbulent flows. *Phys. Rep.* **767–769**, 1–101.

Benavides, S. J. & Alexakis, A. 2017 Critical transitions in thin layer turbulence. *J. Fluid Mech.* **822**, 364–385.

Bernard, D. 1999 Three-point velocity correlation functions in two-dimensional forced turbulence. *Phys. Rev.* E **60** (5), 6184–6187.

https://doi.org/10.1017/jfm.2019.651 Published online by Cambridge University Press

BYRNE, D., XIA, H. & SHATS, M. 2011 Robust inverse energy cascade and turbulence structure in three-dimensional layers of fluid. *Phys. Fluid* **23**, 095109.

BYRNE, D. & ZHANG, J. A. 2013 Height-dependent transition from 3-D to 2-D turbulence in the hurricane boundary layer. *Geophys. Res. Lett.* **40**, 1439–1442.

CELANI, A., MUSACCHIO, S. & VINCENZI, D. 2010 Turbulence in more than two and less than three dimensions. *Phys. Res. Lett.* **104**, 184506.

CHO, J. Y. N. & LINDBORG, E. 2001 Horizontal velocity structure functions in the upper troposphere and lower stratosphere 1. Observations. *J. Geophys. Res.* **106** (D10), 10223–10232.

DEUSEBIO, E., AUGIER, P. & LINDBORG, E. 2014 Third-order structure functions in rotating and stratified turbulence: a comparison between numerical, analytical and observational results. *J. Fluid Mech.* **755**, 294–313.

FRISCH, U. 1995 *Turbulence: the Legacy of A. N. Kolmogorov*. Cambridge University Press.

GALLET, B. & DOERING, C. R. 2015 Exact two-dimensionalization of low-magnetic-Reynolds-number flows subject to a strong magnetic field. *J. Fluid Mech.* **773**, 154–177.

KOLMOGOROV, A. N. 1941 Dissipation of energy in locally isotropic turbulence. *Dokl. Akad. Nauk SSSR* **32**, 16–18.

KRAICHNAN, R. H. 1971 Inertial-range transfer in two- and three-dimensional turbulence. *J. Fluid Mech.* **47**, 525–535.

KRAICHNAN, R. H. 1982 Inertial ranges in two-dimensional turbulence. *Phys. Fluids* **10**, 1417–1423.

KURIEN, S., SMITH, L. & WINGATE, B. 2006 On the two-point correlation of potential vorticity in rotating and stratified turbulence. *J. Fluid Mech.* **555**, 131–140.

LINDBORG, E. 1999 Can the atmospheric kinetic energy spectrum be explained by two-dimensional turbulence? *J. Fluid Mech.* **388**, 259–288.

LINDBORG, E. 2007 Third-order structure function relations for quasi-geostrophic turbulence. *J. Fluid Mech.* **572**, 255–260.

MARINO, R., POUQUET, A. & ROSENBERG, D. 2015 Resolving the paradox of oceanic large-scale balance and small-scale mixing. *Phys. Rev. Lett.* **114**, 114504.

MONIN, A. S. & YAGLOM, A. M. 1975 *Statistical Fluid Mechanics, Volume II: Mechanics of Turbulence*. Dover, (reprinted 2007).

PODESTA, J. J. 2008 Laws for third-order moments in homogeneous anisotropic incompressible magnetohydrodynamic turbulence. *J. Fluid Mech.* **609**, 171–194.

POUQUET, A., MARINO, R., MININNI, P. D. & ROSENBERG, D. 2017 Dual constant-flux energy cascades to both large scales and small scales. *Phys. Rev. Fluids* **29**, 111108.

SESHASAYANAN, K. & ALEXAKIS, A. 2016 Critical behavior in the inverse to forward energy transition in two-dimensional magnetohydrodynamic flow. *Phys. Rev.* E **93**, 013104.

SESHASAYANAN, K., BENAVIDES, S. J. & ALEXAKIS, A. 2014 On the edge of an inverse cascade. *Phys. Rev.* E **90**, 051003(R).

SMITH, K. S., BOCCALETTI, G., HENNING, C. C., MARINOV, I., TAM, C. Y., HELD, I. M. & VALLIS, G. K. 2002 Turbulent diffusion in the geostrophic inverse cascade. *J. Fluid Mech.* **469**, 13–48.

SORRISO-VALVO, L., MARINO, R., CARBONE, V., NOULLEZ, A., LEPRETI, F., VELTRI, P., BRUNO, R., BAVASSANO, B. & PIETROPAOLO, E. 2007 Observation of inertial energy cascade in interplanetary space plasma. *Phys. Res. Lett.* **99**, 115001.

XIE, J.-H. & BÜHLER, O. 2018 Exact third-order structure functions for two-dimensional turbulence. *J. Fluid Mech.* **851**, 672–686.

XIE, J.-H. & BÜHLER, O. 2019 Two-dimensional isotropic inertia–gravity wave turbulence. *J. Fluid Mech.* **872**, 752–783.

YAKHOT, V. 1999 Two-dimensional turbulence in the inverse cascade range. *Phys. Rev.* E **60** (5), 5544–5551.

YOUNG, R. M. B. & READ, P. L. 2017 Forward and inverse kinetic energy cascades in Jupiter's turbulent weather layer. *Nat. Phys.* **13**, 1135–1140.

https://doi.org/10.1017/jfm.2019.651 Published online by Cambridge University Press